Near-infrared co-illumination of fluorescent proteins reduces photobleaching and phototoxicity

Lucie Ludvikova, Emma Simon, Mathieu Deygas, Thomas Panier, Marie-Aude Plamont, Jean Ollion, Alison Tebo, Matthieu Piel, Ludovic Jullien, Lydia Robert, et al.

nature biotechnology

Brief Communication

https://doi.org/10.1038/s41587-023-01893-7

Near-infrared co-illumination of fluorescent proteins reduces photobleaching and phototoxicity

Received: 31 January 2022

Accepted: 30 June 2023

Published online: 03 August 2023

Check for updates

Lucie Ludvikova[1], Emma Simon[1], Mathieu Deygas[2,3], Thomas Panier[4], Marie-Aude Plamont[1], Jean Ollion[5], Alison Tebo[1], Matthieu Piel[2,3], Ludovic Jullien[1], Lydia Robert[4,6] ✉, Thomas Le Saux[1] ✉ & Agathe Espagne[1] ✉

Here we present a method to reduce the photobleaching of fluorescent proteins and the associated phototoxicity. It exploits a photophysical process known as reverse intersystem crossing, which we induce by near-infrared co-illumination during fluorophore excitation. This dual illumination method reduces photobleaching effects 1.5–9.2-fold, can be easily implemented on commercial microscopes and is effective in eukaryotic and prokaryotic cells with a wide range of fluorescent proteins.

The illumination required to excite fluorophores leads to their gradual photodegradation, a phenomenon known as photobleaching. Photobleaching limits the duration and time resolution of experiments and degrades image quality. Although its mechanisms are not fully understood, photobleaching is often assumed to involve the triplet excited state of the fluorophore and its interaction with molecular oxygen, leading to the formation of reactive oxygen species (ROS), which further react with the fluorophore[1–3]. The ROS resulting from fluorophore excitation are, in addition, harmful to cells and contribute to phototoxicity[4].

This picture has inspired several strategies to reduce photobleaching and phototoxicity. Changes in the fluorophore environment, such as oxygen removal, the addition of antioxidants or the use of mixtures of reductants and oxidants to quench the triplet state, have been reported to be helpful[5–9]. These methods are easy to implement and compatible with any imaging technique, but they can have a strong impact on cellular physiology. Other approaches rely on spatial or temporal modulation of the intensity of the (one-color) excitation[10,11], but they are specific to laser scanning microscopies, and their implementation is complex and expensive.

In this study, we explored a different strategy that is easy to implement and causes minimal perturbations to biological samples, namely the use of two-color illumination. It is known that the relaxation of the triplet states of some dyes can be accelerated by light through a photophysical process called reverse intersystem crossing (RISC)[12–14]. RISC is achieved by exciting the dye from its lowest triplet state to a higher triplet state from which it transitions back to singlet excited states before relaxing to the ground state. After the publication of the enhanced green fluorescent protein (EGFP) triplet absorption spectrum, which shows a maximum at 900 nm[15], and the report of RISC in some yellow variants[14,16], we hypothesized that the photobleaching of fluorescent proteins (FPs) under visible light excitation would be reduced by co-illumination with near-infrared (NIR) light. To assess this hypothesis, a sample of purified EGFP immobilized in a polyacrylamide (PAA) gel and continuously illuminated at 470 nm (32 W/cm^2) was co-illuminated at 900 nm (2 kW/cm^2) within a subregion of the field of view. After a few minutes, only the co-illuminated region was still visible (Fig. 1a). We measured a reduced photobleaching (RP) effect of 3.5, defined as the ratio of time-integrated emission in the presence of NIR light to the emission in absence of NIR light (Fig. 1b).

To specify the illumination conditions eliciting the RP effect, we next carried out a series of experiments on EGFP-PAA gels by varying the wavelength of the NIR laser and the intensities of the visible and NIR illuminations. The RP effect increased with NIR light intensity up to

[1]PASTEUR, Département de chimie, École normale supérieure, PSL University, Sorbonne Université, CNRS, Paris, France. [2]Institut Curie, Paris Sciences et Lettres (PSL) Research University, Centre National de la Recherche Scientifique (CNRS), Paris, France. [3]Institut Pierre-Gilles de Gennes, PSL Research University, Paris, France. [4]Sorbonne Université, CNRS, Institut de Biologie Paris-Seine (IBPS), Laboratoire Jean Perrin (LJP), Paris, France. [5]SABILab, Die, France. [6]Université Paris-Saclay, INRAE, AgroParisTech, Micalis Institute, Jouy-en-Josas, France. ✉e-mail: lydia.robert@inrae.fr; thomas.lesaux@ens.psl.eu; agathe.espagne@ens.psl.eu

https://doi.org/10.1038/s41587-023-01893-7

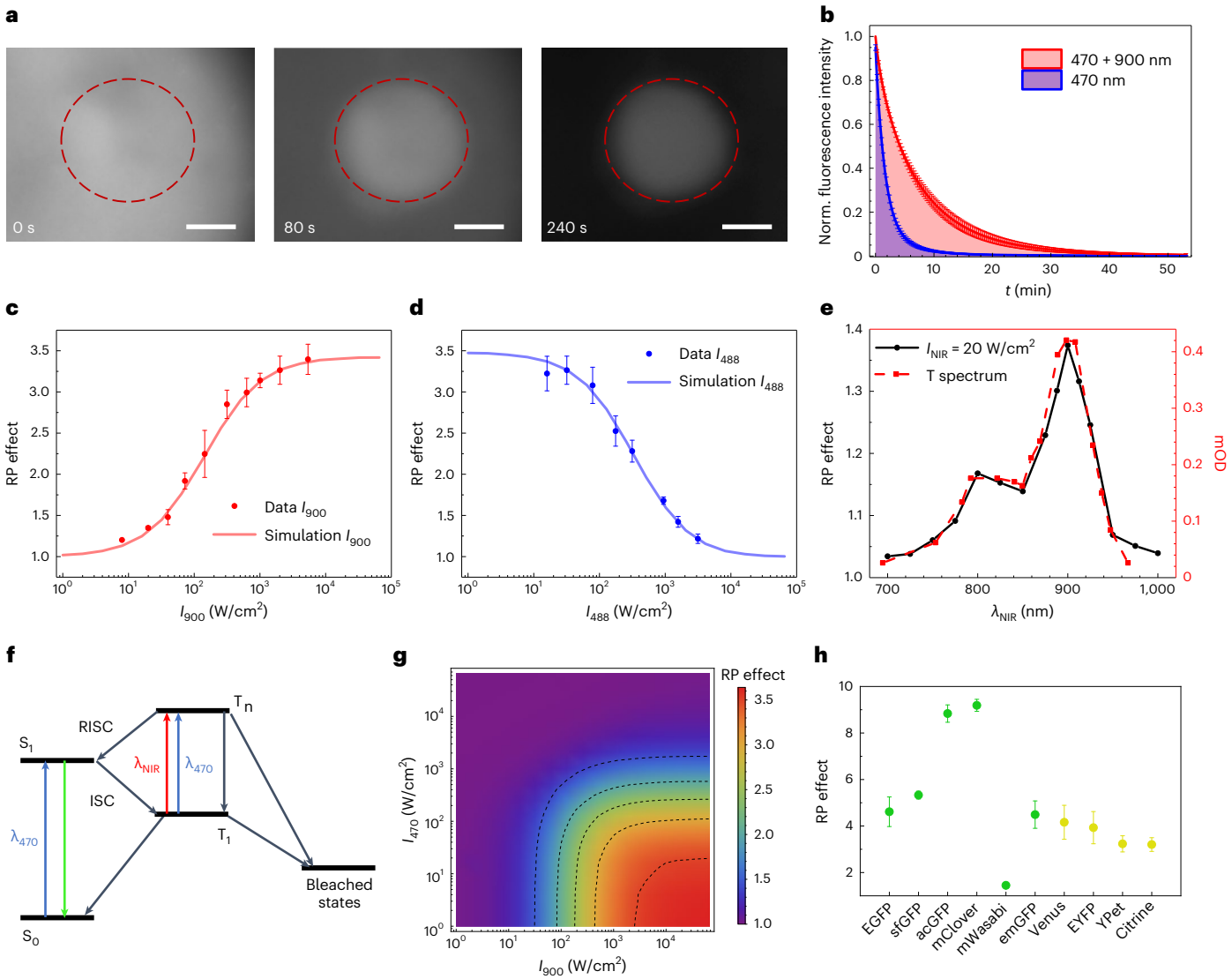

Fig. 1 | Mechanistic investigation of reduced photobleaching. a, Fluorescence images of EGFP immobilized in a PAA gel and illuminated at 470 nm (32 W/cm^2, whole field) and at 900 nm (2 kW/cm^2, red dashed circle). Scale bars, 20 µm. Representative of $n = 4$ replicate experiments. **b**, Photobleaching kinetics of EGFP illuminated solely at 470 nm (blue) or at both 470 nm and 900 nm (red). Values are mean ± s.d. ($n = 4$ samples). **c**,**d**, Dependence of the reduced photobleaching (RP) effect on NIR light intensity I_{900} (**c**; $I_{470} = 32$ W/cm^2) and on visible light intensity I_{488} (**d**; $I_{900} = 2$ kW/cm^2). Values are mean ± s.d. ($n = 3$ samples). Lines are simulations based on the model shown in **f**. **e**, Dependence of the RP effect on the NIR wavelength λ_{NIR}. Black line: measurement performed with $I_{470} = 32$ W/cm^2 and $I_{NIR} = 20$ W/cm^2. Red dashed line: EGFP triplet absorption spectrum from ref. 15. mOD stands for 10^{-3} OD (optical density). **f**, Photophysical model. Triplet T_1, a precursor of bleached states, forms from the bright S_1 state under 470-nm illumination. NIR co-illumination promotes T_1 into the higher triplet T_n from which the fluorophore returns to S_1 by RISC. **g**, RP effect predicted by the model as a function of I_{470} (left axis) and I_{900} (bottom axis). **h**, RP effect for different green and yellow FPs expressed in *E. coli*. $I_{470} = 32$ W/cm^2; $I_{900} = 2$ kW/cm^2. Values are mean ± s.d. ($n = 3$ samples).

~2 kW/cm^2 where it reached a plateau (Fig. 1c) and decreased for visible light intensities higher than ~100 W/cm^2 (Fig. 1d). The action spectrum at low NIR light intensity was found identical to the published triplet absorption spectrum (Fig. 1e), which proves both the involvement of the triplet in a photobleaching pathway of EGFP and the existence of RISC in this FP.

To understand further the mechanisms underlying the RP effect, we constructed a photophysical model describing the transitions between the relevant singlet and triplet states of EGFP (Supplementary Discussion). To account for the decrease of the RP effect at high visible light intensity and its saturation at high NIR light intensity, we had to extend the classical RISC model and consider the non-zero absorption of the lowest triplet state (T_1) at 470 nm and a second photobleaching pathway from the upper triplet state (T_n; Fig. 1f). This model enabled us to satisfactorily simulate the experimental intensity dependencies (Fig. 1c,d). It predicts a maximal RP effect (≥3) for EGFP when visible intensity is lower than 100 W/cm^2 and NIR intensity is higher than 500 W/cm^2 (Fig. 1g).

Then, we assessed the generality of the RP effect among FPs. NIR co-illumination had a beneficial effect for all green and yellow FPs tested (Fig. 1h and Supplementary Fig. 1), with an RP effect ranging from 1.5 to 9.2, likely reflecting slight variations in the photophysical parameters (Supplementary Discussion). The cyan variant ECFP showed, in contrast, no effect in the 700–1,000-nm range (Supplementary Fig. 2), whereas red FPs exhibited a more complex behavior (Supplementary Fig. 3).

Strong RP effects obtained for moderate intensities of visible light suggested that NIR co-illumination could be used to reduce FP

https://doi.org/10.1038/s41587-023-01893-7

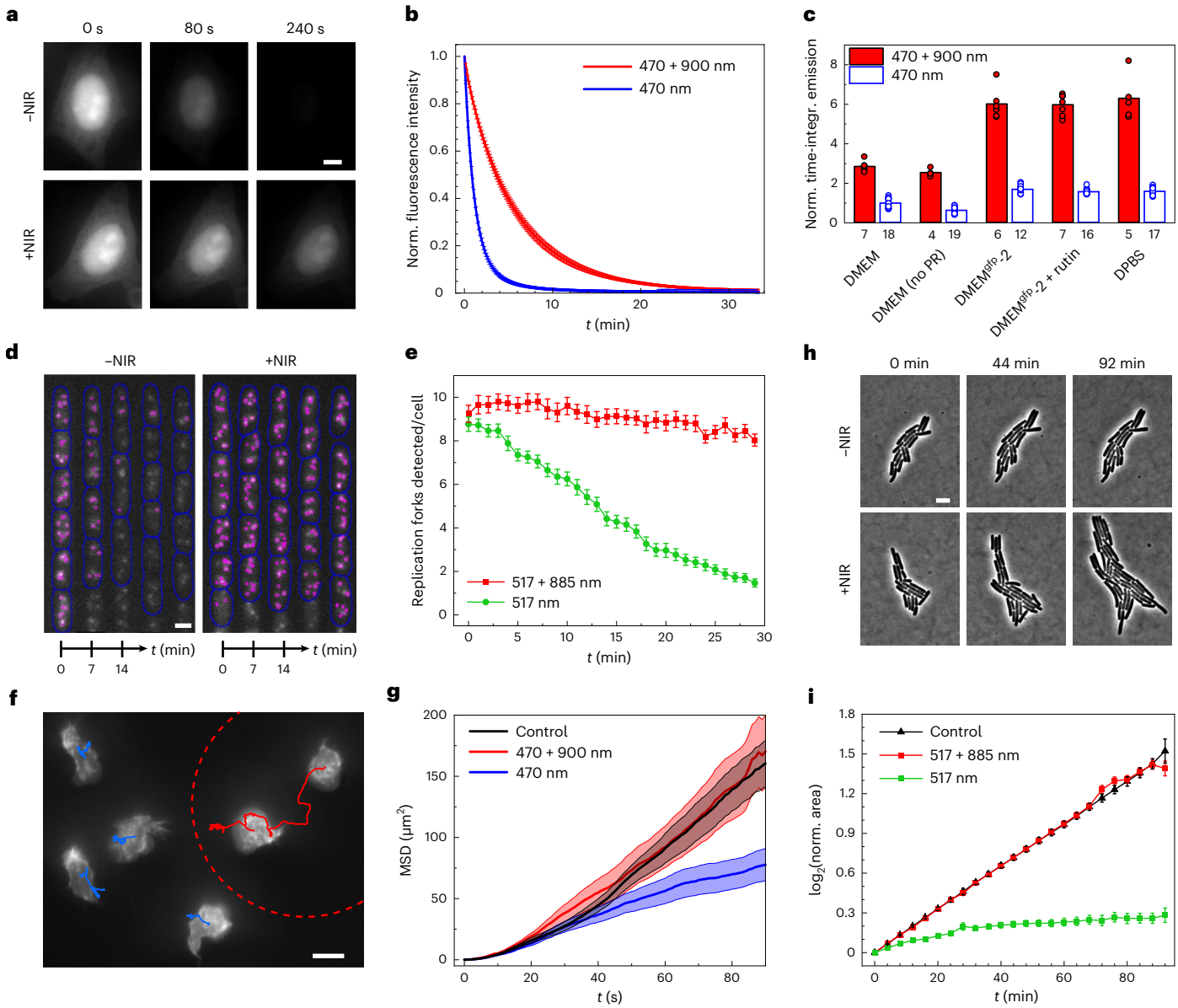

Fig. 2 | NIR co-illumination reduces photobleaching and phototoxicity in eukaryotic and prokaryotic cells. a, Fluorescence images of fixed HeLa cells labeled with EGFP and illuminated at 470 nm alone (top) or combined with 900 nm (bottom). Scale bar, 10 µm. Representative of $n = 3$ replicate experiments. **b**, Photobleaching kinetics of fixed HeLa cells. Values are mean ± s.d. ($n = 12$ cells examined over three samples). **c**, Time-integrated emission of live HeLa cells labeled with EGFP and illuminated at 470 nm alone (white bars) or combined with 900 nm (red bars), in different media. PR, phenol red. All integrals were normalized to that measured in standard DMEM in the absence of NIR light. Dots correspond to individual cells and bar heights to mean. The number of cells is indicated below the bars. **d**, Kymographs of *E. coli* bacteria (blue contours) expressing the DnaN-YPet fusion to mark replisomes (magenta spots). Bacteria growing in the 'mother machine' microfluidic chip at 37 °C were imaged in fluorescence in three *z* planes distant from 350 nm by illumination at 517 nm alone (left) or combined with 885 nm (right). We show the middle plane with replisomes detected by exploiting the three planes. Scale bar, 2 µm. Representative of $n = 2$ replicate experiments. **e**, Number of replisomes detected per cell as a function of time. Values are mean ± s.e.m. ($n = 60$ cells). **f**, Fluorescence image with 5-min cell tracks of primary mouse neutrophils expressing LifeAct-GFP and migrating in a PDMS microchamber at 37 °C under illumination at 470 nm (whole field) and 900 nm (red dashed circle). Scale bar, 10 µm. Representative of $n = 2$ replicate experiments. **g**, Mean squared displacement (MSD) of neutrophils. The control was obtained using minimal 470-nm illumination. Values are mean ± s.e.m. ($n = 32$ cells for 470-nm illumination, $n = 14$ cells for dual illumination and $n = 46$ cells for control). **h**, Phase contrast images showing the growth of YPet-labeled *E. coli* microcolonies on an agarose pad at 37 °C under illumination at 517 nm alone (top) or combined with 885 nm (bottom). Scale bar, 5 µm. Representative of $n = 2$ replicate experiments. **i**, Time evolution of the binary logarithm of the area of the bacterial colonies normalized to their initial area. Values are mean ± s.e.m. ($n = 14$ colonies for 517-nm and dual illumination and $n = 4$ colonies for control, examined over two samples). All illumination conditions are specified in Supplementary Table 1.

photobleaching in live cell imaging using wide-field microscopy (typical intensities ≤1 W/cm^2). As a control, we first performed in situ temperature measurements with a molecular probe[17] and found no significant temperature increase due to NIR light (Supplementary Fig. 4). Next, we implemented NIR co-illumination on a Nikon Eclipse Ti wide-field fluorescence microscope. A straightforward modification of the epifluorescence illuminator to integrate an 885-nm laser diode enabled us to achieve an NIR co-illumination of 0.8 kW/cm^2 over the same field as the visible excitation (Supplementary Fig. 5). As expected, using this setup, we observed a strong RP effect for EGFP and the yellow FP YPet

(Supplementary Fig. 6). We then evaluated the effect of NIR light on FP-labeled biological samples. NIR co-illumination of EGFP expressed in live or fixed HeLa cells or in live bacteria induced a reduction in photobleaching similar to that obtained in vitro (Fig. 2a,b, Supplementary Fig. 7 and Supplementary Video 1). By comparing the photobleaching kinetics of live HeLa cells labeled with EGFP in different media, we found, in addition, that NIR co-illumination in standard DMEM increases the time-integrated emission more than exchanging the medium against vitamin-depleted DMEM^{gfp}-2 (refs. 8,9), which is currently the main available solution to reduce FP photobleaching in live mammalian cells. Both strategies can be combined to obtain an even higher six-fold increase of emission (Fig. 2c and Supplementary Fig. 8).

To further demonstrate that our method can substantially improve in vivo wide-field imaging, we followed fluorescently tagged replisomes (DnaN-YPet) in *Escherichia coli* cells in fast growth conditions (see Methods for details). Many recent studies on the bacterial cell cycle involving replisome visualization have been hampered by the difficulty to detect and track the numerous replisomes present in fast-growing cells[18,19]. Accurate detection and tracking requires imaging several *z* planes at high temporal resolution, which leads to substantial photobleaching of the FP (Supplementary Fig. 9). We found that NIR co-illumination greatly prolongs the visualization of replisomes. As expected, YPet photobleaching under classical one-color excitation led to a rapid decrease in the number of replisomes detected by our analysis software. In contrast, NIR co-illumination enabled us to detect a constant number of ~9 replisomes per cell throughout the cycle (Fig. 2d,e and Supplementary Video 2).

We next reasoned that, by quenching the fluorophore triplet state, NIR co-illumination should also decrease ROS production and, hence, phototoxicity, and we tested this hypothesis in mammalian cells and bacteria. Mammalian cell migration has been shown to be a sensitive readout of phototoxicity[20]. We examined the motility of primary mouse neutrophils expressing LifeAct-GFP under different illumination conditions. Cells illuminated with 20 W/cm^2 of 470-nm light traveled shorter trajectories than minimally illuminated control cells, showing the phototoxic effect of such illumination. As expected, this phototoxicity was substantially reduced by NIR co-illumination (Fig. 2f,g, Supplementary Fig. 10 and Supplementary Video 3). In addition, NIR light led to a substantial reduction of GFP photobleaching (Supplementary Fig. 10). As a second assay, we monitored the growth of FP-labeled *E. coli* microcolonies in the presence and absence of NIR light. Cell proliferation is the standard measure of fitness in bacteria and a well-established criterion for assessing phototoxicity[4]. NIR co-illumination had no effect on phototoxicity for EGFP-labeled bacteria excited at 490 nm, likely because toxicity at this wavelength is mainly caused by endogenous photosensitizers (Supplementary Fig. 11 and Supplementary Note 1). In contrast, we found that NIR co-illumination substantially reduces phototoxicity for YPet-labeled bacteria illuminated at 517 nm. Depending on the exposure time, 517-nm illuminated bacteria hardly grew (Fig. 2h,i and Supplementary Video 4) or grew slower than the non-illuminated control (Supplementary Fig. 12), whereas dual illumination at 517 nm and 885 nm restored a normal growth rate. As expected, FP photobleaching was also substantially reduced by NIR co-illumination in these experiments (Supplementary Fig. 13).

In conclusion, this work shows that the photophysical process of RISC can be exploited to reduce the photobleaching and phototoxicity of FPs in vivo in wide-field imaging, through NIR co-illumination at ~900 nm. This approach can be easily implemented on commercial microscopes, by adding a light source at ~900 nm. Unlike anti-fading reagents and media, it does not require any special preparation of samples before imaging nor the use of a particular culture medium, which makes it compatible with a wide range of biological samples. Beyond wide-field imaging, such NIR co-illumination of FPs could be beneficial for all imaging techniques using visible excitation intensities lower than ~100 W/cm^2.

Online content

Any methods, additional references, Nature Portfolio reporting summaries, source data, extended data, supplementary information, acknowledgements, peer review information; details of author contributions and competing interests; and statements of data and code availability are available at https://doi.org/10.1038/s41587-023-01893-7.

References

1. Stennett, E. M., Ciuba, M. A. & Levitus, M. Photophysical processes in single molecule organic fluorescent probes. *Chem. Soc. Rev.* **43**, 1057–1075 (2014).
2. Acharya, A. et al. Photoinduced chemistry in fluorescent proteins: curse or blessing? *Chem. Rev.* **117**, 758–795 (2017).
3. Duan, C. et al. Structural evidence for a two-regime photobleaching mechanism in a reversibly switchable fluorescent protein. *J. Am. Chem. Soc.* **135**, 15841–15850 (2013).
4. Laissue, P. P., Alghamdi, R. A., Tomancak, P., Reynaud, E. G. & Shroff, H. Assessing phototoxicity in live fluorescence imaging. *Nat. Methods* **14**, 657–661 (2017).
5. Rasnik, I., McKinney, S. A. & Ha, T. Nonblinking and longlasting single-molecule fluorescence imaging. *Nat. Methods* **3**, 891–893 (2006).
6. Vogelsang, J. et al. A reducing and oxidizing system minimizes photobleaching and blinking of fluorescent dyes. *Angew. Chem. Int. Ed.* **47**, 5465–5469 (2008).
7. Cordes, T., Maiser, A., Steinhauer, C., Schermelleh, L. & Tinnefeld, P. Mechanisms and advancement of antifading agents for fluorescence microscopy and single-molecule spectroscopy. *Phys. Chem. Chem. Phys.* **13**, 6699–6709 (2011).
8. Bogdanov, A. M., Bogdanova, E. A., Chudakov, D. M., Gorodnicheva, T. V., Lukyanov, S. & Lukyanov, K. A. Cell culture medium affects GFP photostability: a solution. *Nat. Methods* **6**, 859–860 (2009).
9. Bogdanov, A. M., Kudryavtseva, E. I. & Lukyanov, K. A. Anti-fading media for live cell GFP imaging. *PLoS ONE* **7**, e53004 (2012).
10. Hoebe, R. A., Van Oven, C. H., Gadella, T. W. J., Dhonukshe, P. B., Van Noorden, C. J. F. & Manders, E. M. M. Controlled light-exposure microscopy reduces photobleaching and phototoxicity in fluorescence live-cell imaging. *Nat. Biotechnol.* **25**, 249–253 (2007).
11. Donnert, G., Eggeling, C. & Hell, S. W. Major signal increase in fluorescence microscopy through dark-state relaxation. *Nat. Methods* **4**, 81–86 (2007).
12. Reindl, S. & Penzkofer, A. Higher excited-state triplet-singlet intersystem crossing of some organic dyes. *Chem. Phys.* **211**, 431–439 (1996).
13. Redmond, R. W., Kochevar, I. E., Krieg, M., Smith, G. & McGimpsey, W. G. Excited-state relaxation in cyanine dyes: a remarkably efficient reverse intersystem crossing from upper triplet levels. *J. Phys. Chem. A* **101**, 2773–2777 (1997).
14. Ringemann, C., Schönle, A., Giske, A., von Middendorff, C., Hell, S. W. & Eggeling, C. Enhancing fluorescence brightness: effect of reverse intersystem crossing studied by fluorescence fluctuation spectroscopy. *Chemphyschem* **9**, 612–624 (2008).
15. Byrdin, M., Duan, C., Bourgeois, D. & Brettel, K. A long-lived triplet state is the entrance gateway to oxidative photochemistry in green fluorescent proteins. *J. Am. Chem. Soc.* **140**, 2897–2905 (2018).
16. Peng, B. et al. Optically modulated and optically activated delayed fluorescent proteins through dark state engineering. *J. Phys. Chem. B* **125**, 5200–5209 (2021).
17. Barilero, T., Le Saux, T., Gosse, C. & Jullien, L. Fluorescent thermometers for dual-emission-wavelength measurements: molecular engineering and application to thermal imaging in a microsystem. *Anal. Chem.* **81**, 7988–8000 (2009).

18. Japaridze, A., Gogou, C., Kerssemakers, J. W. J., Nguyen, H. M. & Dekker, C. Direct observation of independently moving replisomes in *Escherichia coli*. *Nat. Commun.* **11**, 3109 (2020).
19. Tiruvadi-Krishnan, S., Mannik, J., Kar, P., Lin, J., Amir, A. & Mannik, J. Coupling between DNA replication, segregation, and the onset of constriction in *Escherichia coli*. *Cell Rep.* **38**, 110539 (2022).
20. Kiepas, A., Voorand, E., Mubaid, F., Siegel, P. M. & Brown, C. M. Optimizing live-cell fluorescence imaging conditions to minimize phototoxicity. *J. Cell Sci.* **133**, jcs242834 (2020).

Methods

Photophysical characterization of the RP effect

Plasmids for bacterial expression of FPs. The plasmid for bacterial expression of emGFP was purchased from Invitrogen (pRSET-EmGFP, ref. V35320). The genes encoding sfGFP, acGFP, mWasabi and mClover were ordered from Integrated DNA Technologies and inserted into the pET28a bacterial expression vector (Novagen) by Gibson assembly using appropriate primers. See Supplementary Table 2 for the sequences of the g-blocks and primers used. The constructs for bacterial expression of EGFP, Venus and mCherry, based on the same pET28a vector, are gifts from Arnaud Gautier (Sorbonne Université) and are described in ref. 21. The constructs for bacterial expression of ECFP and EYFP are based on the pPROEX HTa vector (Invitrogen) and are gifts from Regis Grailhe (Institut Pasteur Korea). The constructs for bacterial expression of Citrine, YPet and mRFP1 are gifts from Robert Campbell, Michael Davidson, Oliver Griesbeck and Roger Tsien[22], Patrick Daugherty and Michael Davidson[23] and Philippe Cluzel[24], respectively (Addgene plasmids 54772, 54860 and 104001).

EGFP expression and purification. His-tagged EGFP was expressed in *E. coli* BL21(DE3) (New England Biolabs) using the pET28a expression vector (Novagen). The bacteria were transformed by electroporation following a standard protocol. Then, 250 ml of TB-kanamycin (50 µg ml^{-1}) was inoculated with an overnight preculture and grown at 37 °C, 220 r.p.m., until the optical density at 600 nm (OD_{600}) reached 0.6 (2–4 h), and then IPTG (1 mM) was added, and the temperature was lowered to 16 °C. After overnight expression, the cells were collected by centrifugation (15 min, 4,700*g*), and then the pellet was washed with 6 ml of PBS and centrifuged again (10 min, 11,000*g*) and then frozen. The pellets were resuspended in lysis buffer (5 ml of PBS, 25 µl of 5 mg ml^{-1} DNase, 50 µl of 100 mM PMSF), sonicated for 5 min and incubated on ice for 2 h. The mixture was centrifuged (11,000*g*, 1 h, 4 °C) to remove cell debris, and the supernatant was incubated overnight at 4 °C with Ni-NTA agarose beads (Sigma-Aldrich) on a rotator mixer. Ni-NTA affinity chromatography was carried out using a Glass Econo-Column (Bio-Rad, 0.7 cm × 20 cm). The beads were washed with PBS buffers containing 30 mM, and then 10 mM imidazole and EGFP was finally eluted with PBS buffer containing 150 mM imidazole. Imidazole was removed by overnight dialysis against PBS buffer using Slide-A-Lyzer Dialysis Cassettes (Thermo Fisher Scientific). The concentration of EGFP solutions was calculated from their absorption spectrum measured on a Cary 300 Scan spectrophotometer (Varian) using a molar absorption coefficient of 55,900 mol^{-1} L cm^{-1} at 488 nm[25,26]. They were aliquoted and stored at −20 °C until use.

EGFP-PAA gels. Next, 21 µl of purified EGFP (40 µM) was mixed with 15 µl of 40% acrylamide/bis-acrylamide (37.5:1 ratio, Sigma-Aldrich) and 0.5 µl of 100× diluted fluorescent beads (FluoSpheres, 0.04 µm, yellow-green, Invitrogen) to facilitate focusing. Polymerization was initiated by 0.1% ammonium persulfate and 0.1% TEMED (*N*,*N*,*N*′,*N*′-tetramethylene-ethylenediamine). The mixture was placed on a coverslip, covered with another coverslip to form a uniform thin layer (~30 µm) and left to cross-link into gel overnight at room temperature.

Bacteria samples for RP effect measurement in different FPs. One colony of *E. coli* BL21 cells expressing the FP of interest was picked from the Petri dish, added to 2 ml of LB-kanamycin (50 µg ml^{-1}) and grown overnight at 37 °C and 220 r.p.m. Then, 3–10 µl of this preculture was spread on a PBS-agarose pad (1% agarose, thickness 0.25 mm) on a coverslip and covered with another coverslip. The samples were left to settle down overnight at room temperature before use.

Optical setup and data acquisition. Photophysical characterizations of the RP effect were performed on an in-house-built wide-field fluorescence microscope equipped with a ×40/0.75 numerical aperture (NA) air objective (Olympus). The 470-nm excitation was delivered over a 200-µm-diameter round spot by an LED at 470 ± 20 nm (Thorlabs, M470L4) filtered through a 479 ± 40-nm interference filter (BrightLine, Semrock) and the NIR co-illumination over a smaller 45-µm-diameter round spot by a laser tunable in the 700–1,000-nm range (Coherent, Mira, operated in continuous-wave mode) (Supplementary Fig. 14a). To measure the dependence of the RP effect on visible intensity, the LED was replaced by a 488-nm laser diode (Omicron, LuxX 488-100) that was overlapped with the NIR laser (45-µm-diameter round spot) to achieve intensities in the 31–5,388-W/cm^2 range (Supplementary Fig. 14b). The emission light was spectrally filtered with an interference filter at 525 ± 30 nm (BrightLine, Semrock). Two dichroic mirrors, FF506-Di03 (BrightLine, Semrock) and 680dcspxr (Chroma, short-pass), were used to separate the emission from the visible and NIR illuminations. An additional short-pass filter (FF02-694/SP-25, Semrock) was placed in front of the camera to eliminate NIR light. The intensities of both illuminations were measured before and after each measurement using a power meter (Thorlabs). Fluorescence images were recorded with an IMX250 CMOS camera (iDS, UI-3080CP-M-GL Rev.2) controlled by µManager 2.0 software. Although both illuminations were continuous, images were taken every 8–60 s (exposure times, 15–50 ms) with the 470-nm LED as excitation source and every 10 ms to 12 s (exposure times, 0.5–15 ms) with the 488-nm laser diode.

Data analysis. The images were first analyzed with Fiji to extract the photobleaching kinetics. The instant fluorescence was taken as the average over selected regions of interest (ROIs). The data were further analyzed in OriginPro 2015. Data measured on FP-labeled cells were background subtracted to remove the contribution from medium autofluorescence, and the fluorescence intensities of all cells were normalized to 1 at $t = 0$. ROIs in EGFP-PAA gel samples were chosen with same initial intensity values. Unless otherwise mentioned, the magnitude of the RP effect was quantified as the ratio of the areas under the photobleaching curves measured with and without NIR co-illumination.

Simulations. Numerical simulations of the photobleaching kinetics of EGFP and the dependence of the RP effect on the intensity of the 470-nm and NIR illuminations, the wavelength of the NIR illumination and the values of different photophysical parameters were performed based on the model of Fig. 1f, using Wolfram Mathematica 12. A complete description of these simulations can be found in the Supplementary Discussion.

Measurement of sample temperature under NIR illumination

The temperature in the presence of the NIR beam was measured using a DNA-based ratiometric fluorescent temperature probe[17]. A 2-mm-thick PDMS spacer (typical medium height in mammalian cell samples) was placed on a coverslip, filled with the probe solution (20 µM in 10 mM HEPES buffer pH 7.5 with 0.1 M NaCl and 2 mM $MgCl_2$) and covered with another coverslip. A calibration curve was first measured in the absence of the NIR beam. The sample was placed on an aluminum block whose temperature was varied between 30 °C and 45 °C using thermoelectric Peltier devices (CP 1.0-63-05L-RTV, Melcor) driven by a MPT1000 temperature controller (Wavelength Electronics) equipped with a TCS610 thermistor (Wavelength Electronics). A 300-µm-thick copper slide with a 2-mm-wide and 3-cm-long slit for observation was coated with vacuum grease and slid between the aluminum block and the sample to improve thermal contact. The sample was excited at 470 nm and imaged in the green and red channels (ET525/36m (Chroma), resp. 628/32 BrightLine (Semrock)) so as to obtain the ratio of green intensity to red intensity as a function of temperature. The temperature of the heating stage was then set at 37 ± 0.2 °C, and new green and red images were measured in the presence of the NIR beam (80-µm diameter, 1.7 kW/cm^2 at 900 nm) to obtain a temperature map. The data were analyzed using Fiji and MATLAB.

HeLa cell experiments

The construct for mammalian expression of EGFP is described in ref. 21. The HeLa cells (from American Type Culture Collection cell line CCL-2) were cultured in DMEM supplemented with phenol red, GlutaMAX I and 10% (v/v) FCS. For microscopic imaging, cells were seeded in poly-lysine-coated 35-mm ibidi µ-dishes (5×10^5 cells per milliliter) and transfected with 2 µg of plasmid DNA for EGFP expression using Lipofectamine 2000 according to the manufacturer's instructions. After 24 h, the cells were washed twice with 1× DPBS, and the medium was exchanged to DMEM (without serum) for live cell imaging, or they were fixed for 20 min at room temperature with 2% paraformaldehyde. For the assessment of EGFP photostability in different media, the medium was exchanged 30 min before imaging, and the samples were left for that time in the incubator. The following media were compared: DMEM with phenol red (Gibco, Thermo Fisher Scientific, 11995065), DMEM without phenol red (Gibco, Thermo Fisher Scientific, 31053028), DPBS (10×, Gibco, Thermo Fisher Scientific, 14200075) and DMEM^{gfp}-2 with and without rutin (Evrogen). Microscopy experiments on HeLa cells were performed with our in-house-built wide-field fluorescence microscope with dual illumination and analyzed with Fiji and OriginPro 2015 in the same way as in vitro experiments (see above).

Neutrophil experiments

Neutrophil purification and culture. Mouse neutrophils were isolated from the bone marrow of healthy 12-week-old C57Bl6/J LifeAct-GFP mice using the MojoSort Mouse Neutrophil Isolation Kit (BioLegend) according to the manufacturer's instructions. Freshly purified mouse neutrophils were cultured overnight in RPMI (Gibco) supplemented with 10% FBS (Euroclone), 50 ng ml^{-1} GM-CSF (Miltenyi Biotec) and 25 mM HEPES (Gibco) at 37 °C with a 5% CO_2 atmosphere. For animal care, we strictly followed the European and French National Regulation for the Protection of Vertebrate Animals used for Experimental and other Scientific Purposes (Directive 2010/63; French Decree 2013-118). The present experiments, which used mouse strains exhibiting non-harmful phenotypes, did not require a project authorization and benefited from guidance of the Animal Welfare Body, Research Center, Institut Curie. Mice were housed under a 12:12 light/dark cycle in a pathogen-free facility with controlled temperature (22 ± 2 °C) and humidity (55% ± 10%). C57Bl6/J LifeAct-GFP mice were a kind gift from Ana Maria Lennon-Dùmenil (Institut Curie).

Preparation of microchambers. Neutrophil motility was assessed with the use of a specific microdevice consisting of a chamber of 4-µm height as previously described[27,28]. In brief, PDMS (RTV615, Neyco) was used to make microchambers from custom-made molds prepared using a standard photolithography technique. The PDMS chamber and a 35-mm glass-bottom dish (FD35-100, WPI) were plasma activated before being bound to each other. The microdevices were then plasma cleaned, coated with 10 µg ml^{-1} fibronectin (Sigma-Aldrich) for 30 min and then washed three times with PBS and incubated 2 h with complete media. Neutrophils were loaded (10^5) in 3-mm holes punched before plasma treatment. The microdevice was gently flooded with complete media, and neutrophils spontaneously migrated in the 4-µm-height confined regions, where their motility was assessed 1 h later.

Data acquisition. Microscopy experiments on neutrophils were performed using our in-house-built fluorescence microscope with dual illumination (see above), equipped with a UI-3080CP-M-GL (IDS GmbH) or an Orca-Flash4.0 V3 (Hamamatsu Photonics KK) camera. The NIR beam, modulated with an SC10 mechanical shutter (Thorlabs), was expanded before being injected into the microscope objective to produce a homogeneous 80-µm-diameter spot at the sample that typically covered 2–3 neutrophils per field of view. The neutrophil dishes were thermostated at 37 °C ± 0.2 °C using the same heating stage as for temperature measurements. To avoid pH drift, cells observed for 30–60 min were returned to the CO_2 incubator for 1–2 h before any re-observation. Cells were imaged for 5 min under weak (0.8 W/cm^2, 200 ms of exposure every 1 s) or strong (20 W/cm^2, 200–400 ms of exposure every 1 s) 470-nm excitation in the presence or absence of 900-nm light (2 kW/cm^2, 200–400 ms of exposure every 1 s).

Neutrophils segmentation and tracking. Image analysis was performed using BACMMAN software[29] (https://github.com/jeanollion/bacmman) that allows automatic cell segmentation and tracking as well as manual curation of both processes. We developed a method for segmentation using a deep neural network (DNN) trained on a very small training set of nine partially annotated images. Our method involves predicting three classes: background, contours and foreground. We found that predicting contours improved the precision of segmentation. See Supplementary Note 2 for details on DNN architecture, training parameters, training set and data augmentation. The cells were then segmented by applying a watershed transform to the predicted probability of the foreground class. Tracking was performed with BACMMAN by integrating the TrackMate[30] implementation of the algorithm by Jaqaman et al.[31], which employs the Hungarian algorithm to solve the linear assignment problem.

The tracking data were analyzed using Python. Cells that left the visible or NIR field during tracking were excluded from the analysis, as were overlapping cells.

Bacterial growth experiments

Sample preparation. The strains used were *E. coli* BL21 expressing EGFP and *E. coli* MG1655 (CGSC 6300) either unlabeled or expressing YPet. All incubation steps were performed at 37 °C under agitation. Cultures were inoculated in LB broth, supplemented with ampicillin (100 µg ml^{-1}) for MG1655-YPet or kanamycin (50 µg ml^{-1}) for BL21-EGFP and incubated overnight. Before plating on a microscope slide, cultures were prepared as follows. Cultures of BL21-EGFP were diluted 200-fold in LB supplemented with kanamycin (50 µg ml^{-1}) and IPTG (100 µM), incubated for 2 h and diluted again 200-fold. Cultures of MG1655 were diluted 200-fold in LB, incubated for 1.5 h and diluted again 200-fold. Cultures of MG1655-YPet were diluted 1,000-fold in M9 Minimal Medium (M9 salts 5× from Sigma-Aldrich diluted to a 1× working solution and supplemented with 2 mM $MgSO_4$) containing casamino acids (0.2%), arabinose (0.2%) and ampicillin (100 µg ml^{-1}) (MMcasa medium), incubated for 3 h and then diluted again four times. The slides were prepared using the following protocol. Low-melting-temperature agarose (20 g L^{-1}) was dissolved into the medium (MMcasa for MG1655-YPet, LB for MG1655, LB supplemented with 50 µg ml^{-1} kanamycin and 100 µM IPTG for BL21-EGFP) by heating. A Gene Frame (Thermo Fisher Scientific) was stuck on a glass slide, and the resulting cavity was filled with the medium containing agarose, covered with a microscope slide and cooled for 2–3 h at room temperature. Then, the slide was removed, and stripes of agarose were removed using a surgical scalpel to leave one small stripe (~5 mm wide), surrounded by air cavities ensuring oxygenation. Then, 2 µl of the bacterial culture was deposited on the slide. Once the liquid was absorbed, the cavity was sealed with a coverslip, and the slide was incubated at 37 °C for several hours before imaging (~2 h for cells growing in LB and ~3 h for cells growing in MMcasa), allowing cells to grow into small microcolonies.

Optical setup, data acquisition and analysis. The bacterial growth experiments were performed with a Nikon Eclipse Ti microscope controlled by NIS software, whose epifluorescence illuminator was modified to deliver dual visible and NIR illumination (Supplementary Fig. 5). In brief, the NIR light source was a fibered 1-W, 885-nm diode laser (RLTMDL-885-1W, Roithner), and the visible light source was an LED (M490L4 or M530L4, Thorlabs). After collimation of the two beams and expansion of the NIR beam, they were combined using a short-pass dichroic mirror (DMSP805R, Thorlabs) inserted in a filter cube, which

replaced the main body of the illuminator. To reflect both the NIR and visible beams to the sample and collect the fluorescence signal from EGFP or YPet, we equipped a filter cube of the microscope turret with appropriate combinations of a dichroic mirror and a band-pass emission filter (T495lpxr + ET525/50m for EGFP or ZT514rdc + ET545/40m for YPet, all from Chroma). We placed an additional short-pass filter (FESH0650, Thorlabs) below the filter turret to protect the camera from residual NIR light. The objective was a Plan APO ×100 immersion objective (NA 1.4). To assess phototoxicity and photobleaching, growing microcolonies either unlabeled or expressing EGFP or YPet were exposed to blue light (490 nm, 0.5 W/cm^2) or green light (517 nm, 1.2 W/cm^2), respectively, in the presence or absence of NIR co-illumination (885 nm, 0.8 kW/cm^2). Their growth at 37 °C was followed by phase contrast imaging and fluorescence imaging (for FP-labeled bacteria). The data were analyzed with Fiji and OriginPro 2015 in the same way as in vitro data (see above). The areas of the microcolonies were extracted from phase contrast images using Fiji.

Experiments on replisomes

The strain was obtained by transduction of the YPet-DnaN allele[32] (fluorescent fusion of the β-subunit of the DNA polymerase, kind gift from Sven van Teeffelen) into *E. coli* MG1655. An overnight culture in LB medium was loaded into the 'mother machine' microfluidic chip[33]. Fabrication of the chip and cell loading are explained in detail in ref. 34. A flow of 2 ml h^{-1} of LB medium supplemented with 0.1 mg ml^{-1} BSA was delivered to the cells using a PHD ULTRA syringe pump (Harvard Apparatus), allowing fast growth of the cells (~22 min doubling time; an average number of ~10 replisomes per cell is expected in these conditions[35]). The chip was installed on our Nikon Eclipse Ti microscope, modified for dual illumination as explained above and thermostated at 37 °C. Image acquisition began after 4 h of incubation, when cells had reached balanced, exponential growth. Three images corresponding to three different focal planes, distant from 350 nm, were taken every minute, with 300-ms exposure time. Replisomes were segmented using BACMMAN software[29] (https://github.com/jeanollion/bacmman) with the same method used to detect fluorescent foci as in ref. 36. This method detects spots on a criterion based on both the intensity value and the Laplacian transform value. We optimized thresholds so that spots are well detected at the first frame and used the same thresholds for the whole movie in both conditions with and without NIR.

Reporting summary

Further information on research design is available in the Nature Portfolio Reporting Summary linked to this article.

Data availability

The data that support the findings of this study are available at https://doi.org/10.5281/zenodo.8069922.

Code availability

BACMMAN software used to analyze the replisome and neutrophil experiments is available at https://github.com/jeanollion/bacmman/. The code developed for neutrophil segmentation (deep learning model, training procedure and associated documentation) is available at https://github.com/jeanollion/pix_mclass.

References

21. Plamont, M. A. et al. Small fluorescence-activating and absorption-shifting tag for tunable protein imaging in vivo. *Proc. Natl Acad. Sci. USA* **113**, 497–502 (2016).
22. Griesbeck, O., Baird, G. S., Campbell, R. E., Zacharias, D. A. & Tsien, R. Y. Reducing the environmental sensitivity of yellow fluorescent protein. Mechanism and applications. *J. Biol. Chem.* **276**, 29188–29194 (2001).
23. Nguyen, A. W. & Daugherty, P. S. Evolutionary optimization of fluorescent proteins for intracellular FRET. *Nat. Biotechnol.* **23**, 355–360 (2005).
24. Balleza, E., Kim, J. M. & Cluzel, P. Systematic characterization of maturation time of fluorescent proteins in living cells. *Nat. Methods* **15**, 47–51 (2018).
25. Zimmer, M. Green fluorescent protein (GFP): applications, structure, and related photophysical behavior. *Chem. Rev.* **102**, 759–781 (2002).
26. Tsien, R. Y. The green fluorescent protein. *Annu. Rev. Biochem.* **67**, 509–544 (1998).
27. Vargas, P., Terriac, E., Lennon-Dumenil, A. M. & Piel, M. Study of cell migration in microfabricated channels. *J. Vis. Exp.* **21**, e51099 (2014).
28. Sormendi, S. et al. HIF2α is a direct regulator of neutrophil motility. *Blood* **137**, 3416–3427 (2021).
29. Ollion, J., Elez, M. & Robert, L. High-throughput detection and tracking of cells and intracellular spots in mother machine experiments. *Nat. Protoc.* **14**, 3144–3161 (2019).
30. Tinevez, J. Y. et al. TrackMate: an open and extensible platform for single-particle tracking. *Methods* **115**, 80–90 (2017).
31. Jaqaman, K. et al. Robust single-particle tracking in live-cell time-lapse sequences. *Nat. Methods* **5**, 695–702 (2008).
32. Reyes-Lamothe, R., Sherratt, D. J. & Leake, M. C. Stoichiometry and architecture of active DNA replication machinery in *Escherichia coli*. *Science* **328**, 498–501 (2010).
33. Wang, P. et al. Robust growth of *Escherichia coli*. *Curr. Biol.* **20**, 1099–1103 (2010).
34. Robert, L., Ollion, J. & Elez, M. Real-time visualization of mutations and their fitness effects in single bacteria. *Nat. Protoc.* **14**, 3126–3143 (2019).
35. Zaritsky, A., Wang, P. & Vischer, N. O. E. Instructive simulation of the bacterial cell division cycle. *Microbiology (Reading)* **157**, 1876–1885 (2011).
36. Robert, L., Ollion, J., Robert, J., Song, X., Matic, I. & Elez, M. Mutation dynamics and fitness effects followed in single cells. *Science* **359**, 1283–1286 (2018).

Acknowledgements

This work was supported by the Agence Nationale de la Recherche (ANR-19-CE29-0003 (dISCern), ANR-19-CE11-0005 (HIGHLIGHT), ANR-19-CE35-0003 (TRANSMUTATOR), ANR-10-INBS-04 (France Bioimaging), ANR-11-EQPX-0029 (Morphoscope2), ANR-10-LABX-31 (IPGG) and ANR-10-IDEX-0001-02 (PSL)), the Région Île-de-France (DIM ELICIT), CNRS, Sorbonne Université (Emergence 2019-2020 LIGHTNING) and Ecole Normale Supérieure. We thank S. Vriz, M. Volovitch, Z. Gueroui and N. Peyriéras for discussions.

Author contributions

A.E. supervised the work and designed the experiments, with L.L., L.R. and T.L.S. L.L. carried out the mechanistic study of reduced photobleaching (experiments and numerical simulations) and the experiments on HeLa cells. E.S. carried out and analyzed neutrophil experiments and temperature measurements. L.R. carried out the experiments on replisomes and bacterial growth. T.L.S. built the in-house microscope with dual illumination. M.D. designed the neutrophil experiments, with M.P., and prepared the samples. T.P. implemented NIR co-illumination on the Nikon microscope. M.-A.P. prepared HeLa cell samples. J.O. developed the software for neutrophil segmentation and tracking. A.T. constructed the bacterial expression vectors for green FPs. L.J. contributed to photophysical modeling. A.E., L.L. and L.R. wrote the manuscript, with input from all authors.

Competing interests

A patent application has been filed relating to aspects of the work described in this manuscript. The following authors are listed on the patent: A.E., L.L., L.R., T.L.S. and L.J. J.O. is a freelance bioimage analyst. The remaining authors declare no competing interests.

Additional information

Supplementary information The online version contains supplementary material available at https://doi.org/10.1038/s41587-023-01893-7.

Correspondence and requests for materials should be addressed to Lydia Robert, Thomas Le Saux or Agathe Espagne.

Peer review information *Nature Biotechnology* thanks Ilaria Testa and the other, anonymous, reviewer(s) for their contribution to the peer review of this work.

nature research

Corresponding author(s): Agathe Espagne
Thomas Le Saux
Lydia Robert

Last updated by author(s): Jun 29, 2023

Reporting Summary

Nature Research wishes to improve the reproducibility of the work that we publish. This form provides structure for consistency and transparency in reporting. For further information on Nature Research policies, see our Editorial Policies and the Editorial Policy Checklist.

Statistics

For all statistical analyses, confirm that the following items are present in the figure legend, table legend, main text, or Methods section.

n/a	Confirmed	
☐	☒	The exact sample size (*n*) for each experimental group/condition, given as a discrete number and unit of measurement
☐	☒	A statement on whether measurements were taken from distinct samples or whether the same sample was measured repeatedly
☒	☐	The statistical test(s) used AND whether they are one- or two-sided *Only common tests should be described solely by name; describe more complex techniques in the Methods section.*
☒	☐	A description of all covariates tested
☐	☒	A description of any assumptions or corrections, such as tests of normality and adjustment for multiple comparisons
☐	☒	A full description of the statistical parameters including central tendency (e.g. means) or other basic estimates (e.g. regression coefficient) AND variation (e.g. standard deviation) or associated estimates of uncertainty (e.g. confidence intervals)
☒	☐	For null hypothesis testing, the test statistic (e.g. *F*, *t*, *r*) with confidence intervals, effect sizes, degrees of freedom and *P* value noted *Give P values as exact values whenever suitable.*
☒	☐	For Bayesian analysis, information on the choice of priors and Markov chain Monte Carlo settings
☒	☐	For hierarchical and complex designs, identification of the appropriate level for tests and full reporting of outcomes
☒	☐	Estimates of effect sizes (e.g. Cohen's *d*, Pearson's *r*), indicating how they were calculated

Our web collection on statistics for biologists contains articles on many of the points above.

Software and code

Policy information about availability of computer code

Data collection	Fluorescence data aimed at the mechanistic investigation of reduced photobleaching and its quantification in different samples (Fig. 1 a-e and h and Fig. 2 a-c), neutrophil data (Fig. 2 f-g) and temperature data shown in SI were collected using a home-built microscope equipped with a camera controlled by µManager 2.0. Fluorescence and phase-contrast images of bacteria (Fig. 2 d-e and h-i) were acquired using a Nikon microscope controlled by NIS software.
Data analysis	Photobleaching kinetics and the areas of growing bacterial microcolonies were extracted from the fluorescence or phase-contrast images using Fiji (ImageJ 1.53t). Further data analysis was performed with OriginPro 2015. Photophysical simulations were performed with Wolfram Mathematica 12. Temperature data were analyzed using Fiji (ImageJ 1.53t) and Matlab R2022a. Data on E. coli replisomes were analyzed with the BACMMAN software which is already published. Neutrophils were segmented and tracked using BACMMAN and further analysis was carried out with Python 3.10.

For manuscripts utilizing custom algorithms or software that are central to the research but not yet described in published literature, software must be made available to editors and reviewers. We strongly encourage code deposition in a community repository (e.g. GitHub). See the Nature Research guidelines for submitting code & software for further information.

Data

Policy information about availability of data

All manuscripts must include a data availability statement. This statement should provide the following information, where applicable:

- Accession codes, unique identifiers, or web links for publicly available datasets
- A list of figures that have associated raw data
- A description of any restrictions on data availability

The data that support the findings of this study are available at: https://doi.org/10.5281/zenodo.8069922.

Field-specific reporting

Please select the one below that is the best fit for your research. If you are not sure, read the appropriate sections before making your selection.

☒ Life sciences ☐ Behavioural & social sciences ☐ Ecological, evolutionary & environmental sciences

For a reference copy of the document with all sections, see nature.com/documents/nr-reporting-summary-flat.pdf

Life sciences study design

All studies must disclose on these points even when the disclosure is negative.

Sample size	Sample sizes are given in the figure legends. No statistical method was used to pre-determine them. They were experimentally limited by 3 factors: the impossibility of tracking multiple fields of view in parallel with the manual stage of our in-house microscope, the limited area illuminated by the NIR laser which typically covered only 1 to 3 mammalian cells at a time, and the duration of around 30 min required to photobleach EGFP completely. Taking these limitations into account, we chose sample sizes that were sufficient to show significant differences in photobleaching or phototoxicity in the different illumination conditions or imaging media tested, as indicated by the error bars.
Data exclusions	No data were excluded.
Replication	The experiment in Fig. 1a-b was performed in quadruplicate and those in Fig. 1c-d and Fig. 1h in triplicate. The experiment in Fig. 2a-b was performed in triplicate, that in Fig. 2c in quadruplicate and those in Fig. 2d-e, Fig. 2f-g and Fig. 2h-i in duplicate. All attempts at replication were successful. The consistency between results obtained in two different laboratories (PASTEUR and LJP) with different setups and light sources also supports the reproducibility of our experimental findings.
Randomization	Samples allocation into experimental groups was random. Fields of view in EGFP-PAA gels were randomly chosen to test each illumination condition. Live HeLa cells samples were randomly assigned to the different imaging media. Bacterial and mammalian cells exposed to different illumination conditions were randomly chosen within the samples.
Blinding	The same data acquisition and analysis protocols were applied to all samples regardless of their group. Blinding was not possible because sample preparation and data acquisition and analysis were performed by the same person.

Reporting for specific materials, systems and methods

We require information from authors about some types of materials, experimental systems and methods used in many studies. Here, indicate whether each material, system or method listed is relevant to your study. If you are not sure if a list item applies to your research, read the appropriate section before selecting a response.

Materials & experimental systems

n/a	Involved in the study
☒	☐ Antibodies
☐	☒ Eukaryotic cell lines
☒	☐ Palaeontology and archaeology
☐	☒ Animals and other organisms
☒	☐ Human research participants
☒	☐ Clinical data
☒	☐ Dual use research of concern

Methods

n/a	Involved in the study
☒	☐ ChIP-seq
☒	☐ Flow cytometry
☒	☐ MRI-based neuroimaging

Eukaryotic cell lines

Policy information about cell lines

Cell line source(s)	Hela from ATCC, cell line CCL-2, lot number 63226283
Authentication	The cell line was authenticated by STR profiling.
Mycoplasma contamination	The cell line tested negative for mycoplasma contamination.
Commonly misidentified lines (See ICLAC register)	No misidentified cell lines were used.

Animals and other organisms

Policy information about studies involving animals; ARRIVE guidelines recommended for reporting animal research

Laboratory animals	C57Bl6/J LifeaAct-GFP mice from healthy 12-week-old males.
Wild animals	The study did not involve wild animals.
Field-collected samples	The study did not involve samples collected from the field.
Ethics oversight	The present experiments, which used mouse strains exhibiting non-harmful phenotypes, did not require a project authorization and benefited from guidance of the Animal Welfare Body, Research Centre, Institut Curie.

Note that full information on the approval of the study protocol must also be provided in the manuscript.